UC Riverside
UC Riverside Previously Published Works

Title

Controllable direction of liquid jets generated by thermocavitation within a droplet.

Permalink

https://escholarship.org/uc/item/2k24d063

Journal

Applied Optics, 56(25)

ISSN

0003-6935

Authors

Padilla-Martinez, JP
Ramirez-San-Juan, JC
Berrospe-Rodriguez, C
et al.

Publication Date

2017-09-01

DOI

10.1364/ao.56.007167

Peer reviewed

applied optics

Controllable direction of liquid jets generated by thermocavitation within a droplet

J. P. Padilla-Martinez,[1,]* J. C. Ramirez-San-Juan,[2] C. Berrospe-Rodriguez,[2] N. Korneev,[2]
G. Aguilar,[3] P. Zaca-Moran,[1] and R. Ramos-Garcia[2]

[1]*Instituto de Ciencias, Benemérita Universidad Autónoma de Puebla, Puebla 72050, Mexico*
[2]*Departamento de óptica, Instituto Nacional de Astrofísica, Óptica y Electrónica, Puebla 7200, Mexico*
[3]*Department of Mechanical Engineering, University of California Riverside, Riverside, California 92521, USA*
*Corresponding author: juan.padilla@correo.buap.mx

A high-velocity fluid stream ejected from an orifice or nozzle is a common mechanism to produce liquid jets in inkjet printers or to produce sprays among other applications. In the present research, we show the generation of liquid jets of controllable direction produced within a sessile water droplet by thermocavitation. The jets are driven by an acoustic shock wave emitted by the collapse of a hemispherical vapor bubble at the liquid-solid/substrate interface. The generated shock wave is reflected at the liquid-air interface due to acoustic impedance mismatch generating multiple reflections inside the droplet. During each reflection, a force is exerted on the interface driving the jets. Depending on the position of the generation of the bubble within the droplet, the mechanical energy of the shock wave is focused on different regions at the liquid-air interface, ejecting cylindrical liquid jets at different angles. The ejected jet angle dependence is explained by a simple ray tracing model of the propagation of the acoustic shock wave inside the droplet.   © 2017 Optical Society of America

OCIS codes: (350.5340) Photothermal effects; (350.7420) Waves.

https://doi.org/10.1364/AO.56.007167

1. INTRODUCTION

The liquid jets and droplet production have become subject of several studies due to their practical importance in several technical areas such as gasoline combustion [1], drug delivery [2,3], coating [4], inkjet printing [5], water waveguide [6], microelectronics cooling [7,8], and others. Commonly, the liquid jets and their disintegration into droplets are obtained by various types of nozzles, orifices, or apertures modified to control the rate of flow, speed, mass, pressure, the shape of the stream that passes through them, and the direction [9]. When the nozzle is circular, the ejected liquid flow forms a cylindrical column [9], which eventually becomes unstable and breaks up into droplets due to surface tension. This breaking is associated with the Rayleigh–Plateau (R-P) instability, which dictates the maximal length L at which a liquid column of radius r will break up. This relationship is known as the aspect ratio $\Lambda = L/2r$. In weightless conditions, when the liquid column's length exceeds its circumference ($\Lambda > \pi$), it breaks up into droplets.

In the last decade, several methods have been implemented to generate liquid jets without the use of nozzles to achieve aspect ratios $\Lambda > \pi$ [10–16]. For example, it was possible to form a liquid column (1 to 2 cm in length, corresponding to $\Lambda \sim 5$) using surface acoustic waves (SAWs) that propagate along the surface of a substrate until they refract from a hemispherical liquid droplet (placed on the substrate's surface) at an angle known as the Rayleigh angle. This refraction causes a deformation of the droplet and consequently the formation of a liquid jet [10]. SAWs are not the only way to produce liquid jets on a hemispherical liquid droplet. High-speed jets (up to 200 m/s) can also be induced by focusing acoustic waves on the liquid-air interface causing the formation of cavitation bubbles [17]. These acoustic waves are produced under very special conditions, i.e., by using a light-to-sound converter, which consists of a transparent concave lens coated with a composite of carbon-nanotubes embedded in a polymer. In this work, two types of liquid jets were reported, primary slow jets caused by initial bubble and secondary fast jets produced by bubble collapse. An excellent review about microfluidics driven via acoustics and ultrasonic can be found in [18].

Other techniques involve the use of short laser pulses [12–16,19–22] or a spark discharge [23] to create cavitation bubbles within a liquid, droplets, or thin films to produce liquid jets or spray. Among the techniques that use short laser pulses we can mention the laser-induced forward transfer (LIFT) technique [24–28]. In LIFT, a pulsed laser is focused through a transparent (solid or liquid) substrate (donor) and

absorbed in a metallic thin film. As a result of the strong absorption, a high-pressure vapor bubble is created and expands deforming the film and expelling the material. In the case of liquid jets, they are formed by the symmetric flow of fluid toward the pole of the liquid sheet created between the bubble and the substrate, where they generate a pressure maximum that forces the fluid toward those regions. A counter jet is formed and directed toward the bubble, which eventually is deformed taking a toroidal shape. These results were predicted by numerical simulations [29]. The jets reported in [24] are unidirectional; however, later experiments showed that by introducing a second pulsed laser in the LIFT technique, a tilting on one of the jets can be induced in a controlled way [25]. The maximum tilt angle reported was approximately of 15°.

In recent years, capillary tubes have been used to generate microjets with velocities of up to 850 m/s [30]. In this case, a nanosecond pulsed laser is focused inside the liquid-filled capillary to create a vapor bubble near the lower wall of the capillary. The hypothesis about the jet formation is based on the collision of the shockwave caused by the nearly instantaneous vaporization upon the free surface of the liquid [30]. More recently, a microfluidic device was designed and built for the generation of liquid jets produced by thermocavitation [31]. This device consists in a microchamber where cavitation is created connected to a microchannel for jet generation. The microchamber is filled with a highly absorbent solution to the operation wavelength to create a vapor bubble, which rapidly expands displacing the liquid outside the device through the channel [31]. In both cases (capillary and microchamber), the liquid jets are unidirectional.

The use of a continuous wave (CW) laser focused into a hemispherical droplet of highly absorbing liquid has proven to be an alternative technique to produce liquid jets, eliminating the use of nozzles, capillaries, or microcavities. The liquid jets produced by this method are driven by an acoustic shock wave (ASW) emitted at the collapse of a vapor bubble within the droplet contrary to short-pulsed laser-induced cavitation whose dynamic is determined by the bubble [32]. It was shown that the bubble produced by CW lasers is always in contact with the substrate (glass) due to the large optical absorption of the overlaying droplet. The propagation of the ASW was simulated using a ray tracing model as point source originated at the substrate [32]. The simulation shows that the ASW is reflected by the droplet's surface due to an acoustic impedance mismatch ($R = 99.99$) between the solution and air; i.e., the interface acts as a perfect mirror, reflecting the ASW toward the point where it was emitted. However, for the second reflection (glass-liquid interface) only 40% of the ASW is focused at the liquid-air interface; nevertheless, its amplitude is still large enough to drive the dynamic of the liquid columns. A study on the aspect ratio ($\Lambda = L/2r$) was performed in these liquid jets (unidirectional) as a function of the laser power, beam focus position, and droplet's volume [32]; however, no liquid jets of controllable direction were reported.

In the present study, vapor bubbles generated by thermocavitation [32–35] were formed over the substrate-liquid interface, and the resulting reflected ASW was focused at different regions on the upper part of the droplet, ejecting quasi-cylindrical liquid columns at different angles. The control over the liquid column's length and consequently its aspect ratio Λ was controlled by adjusting the vapor bubble's size, which depends on the laser intensity, the beam focus position, and the droplet's volume [32]. Our experimental results about the ejection angle are explained by a simple ray tracing optic model of the propagation of the ASW inside the droplet. Therefore, thermocavitation induced in absorbing droplets could lead to an alternative jet and droplet generator, where the column's length and ejection angle can be readily controlled, opening the possibility for new practical applications.

2. EXPERIMENTAL DESCRIPTION

A saturated solution of copper nitrate ($CuNO_4$) dissolved in water was used as a medium where thermocavitation was induced. Its physical properties are as follows: a high absorption coefficient ($\alpha = 189$ cm^{-1} and penetration length ~ 53 μm) exists at the operating wavelength ($\lambda = 810$ nm) [36]; the density and viscosity of the solution is approximately twice and fivefold of water ($\rho_{sol} \approx 2\rho_{wat}$ and $\mu_{sol} \sim 5\mu_{water}$), respectively [32]; and the surface tension was measured as $\sigma \sim 0.088$ N/m, which is close to the water-alone surface tension ($\sigma_{water} \sim 0.072$ N/m) [32].

A 5 μL $CuNO_4$ droplet was gently deposited on a clean, untreated glass microscope slide (1 mm thickness) and confined by a thin ring-shaped plastic sticker with an inner diameter of 5 mm and ~ 100 μm in thickness, as shown in Fig. 1(a). The laser beam was collimated and focused with a microscope objective ($f = 8$ mm), sitting under the microscope slide. The beam waist at the focus is $w_0 \sim 10$ μm, and the Rayleigh distance is $z_0 \sim 387$ μm. The microscope slide is placed on a 3D translation stage to displace it transversally (x, y) to focus in different positions of the droplet or along the propagation distance z to change the heated volume. The coordinate (0, 0, 0) corresponds to the beam focus placed at the glass-solution interface and centered in the droplet, as shown in Fig. 1(a).
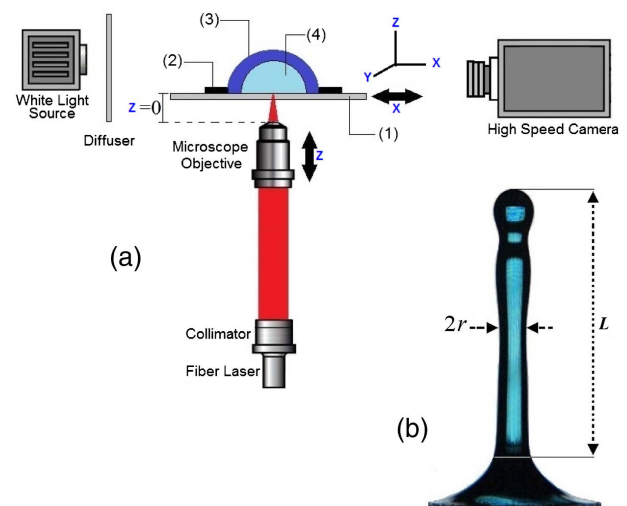
Fig. 1.   (a) Experimental setup for the analysis of liquid jets produced by thermocavitation within a droplet of $CuNO_4$ solution. (1) Microscope slide, (2) ring-shaped plastic sticker, (3) droplet, and (4) vapor bubble. (b) Liquid column.

Owing to the radial symmetry of the droplet, we fixed $y = 0$, and only the positions x and z were adjusted. In this work, two sets of experiments were performed: (i) the laser focus placed at $(0, 0, z)$, where z was varied from –200 to 500 μm, and (ii) the laser focus placed at $(x, 0, 200 \text{ μm})$, where x was varied from –900 to 0 μm.

For these experiments, the laser power was fixed at 580 mW, and the bubble radius was controlled by displacing the beam focus in the z direction [35]. The beam waist at any other distance can be calculated by using the expression $w(z) = w_0(1 + (z/z_o)^2)^{1/2}$. To obtain a single cavitation event, the exposition time was set to ~40 ms. To record the evolution of the vapor bubble inside the droplet and the liquid jet formed after the bubble collapse, a high-speed video camera (Phantom V7.1) was used. The system was illuminated with a white light source almost perpendicular to the laser beam direction. Figure 1(b) shows an example of a liquid jet emerging from the droplet. Its length L and its diameter $2r$ are measured before it breaks up into droplets, determining in this way its aspect ratio Λ.

3. EXPERIMENTAL RESULTS

A. Vapor Bubble Formation and Liquid Jet Evolution

Figure 2 shows the evolution of the vapor bubble created within the droplet during laser exposure starting with the
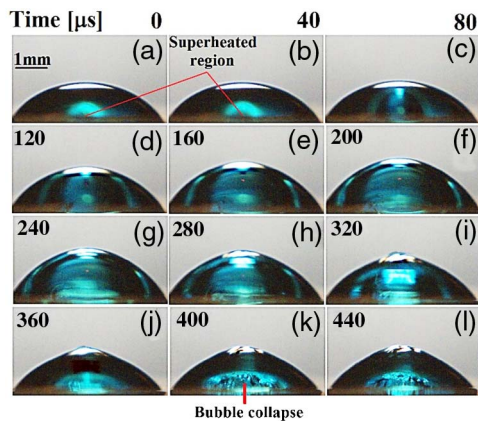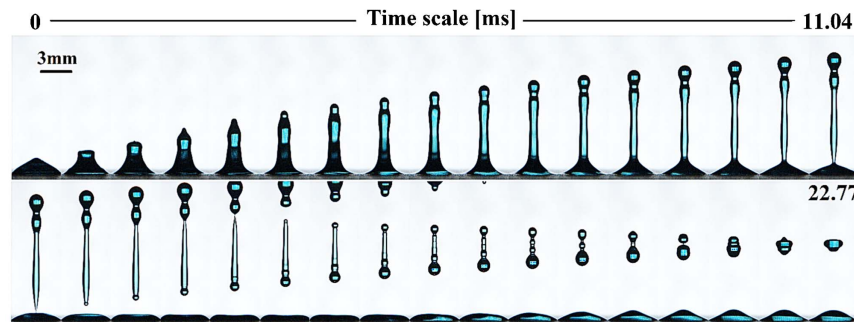

Fig. 2. (See Visualization 1) Formation and evolution of a vapor bubble created inside a droplet (5 μL volume) using a CW laser. The laser focus was placed at the position (0, 0, 0).

5 μL sessile droplet deposited on the ring-shaped plastic container [Fig. 2(a)]. The laser focus was placed on the glass-liquid interface at (0, 0, 0). The laser beam is strongly absorbed by the solution near the interface glass-liquid producing a superheated region [Figs. 2(a) and 2(b)] that undergoes an explosive phase transition [37–40] and, consequently, the formation of a fast-expanding vapor bubble [Fig. 2(c)]. The vapor bubbles produced by this method are commonly termed as thermocavitation bubbles. Further details concerning thermocavitation and its dynamics can be found in [32,34,35,41–44]. The laser-induced bubble is always in contact with the substrate taking a hemispherical shape. The bubble reaches its maximum radius ($r_{max} \sim 1.8$ mm) in approximately 200 μs [Fig. 2(g)] and then collapses in 200 μs [Fig. 2(k)].

At the bubble collapse, a strong ASW is emitted, which propagates within the droplet at a speed of ~1800 m/s reaching the water-air interface in only ~0.5 μs [32]. Owing to the acoustic impedance mismatch between the water and air, the fraction of the incident wave that is reflected is $R \sim 99.9\%$ generating multiple reflections inside the droplet. In each reflection part of the energy of the ASW is lost and eventually it dies off. Because of the droplet curvature, the reflected wavefront is curved, and after the second reflection at the glass-water interface, the ASW is focused around the center of the droplet (liquid-air interface) deforming its surface. If its amplitude is strong enough, a liquid jet may be formed driven by momentum transfer whose speed and length depends on the amplitude of the ASW (Fig. 3).

Figure 3 shows the temporal evolution of a liquid jet generated under the same parameters and conditions of the experiment described in Fig. 2 but recording it over a much longer time scale. The first image in Fig. 3 (time = 0) corresponds to the vapor bubble's collapse [Fig. 2(k)]. Tens of microseconds after the collapse, a cylindrical liquid column is ejected from the upper part of the droplet. The speed of the head of the column at the beginning of its formation is ~1.27 m/s, and after ~11.5 ms the liquid column detaches from the droplet forming a liquid column with two droplets at the front end. The liquid column continues moving upward due to its inertia. Eventually, surface tension causes separation of the column and the formation of a droplet on the lower part of the column. This detached column undergoes oscillations and coalesces into a single droplet. The direction of the jet coincides with the laser beam propagation direction; i.e., it is perpendicular to the
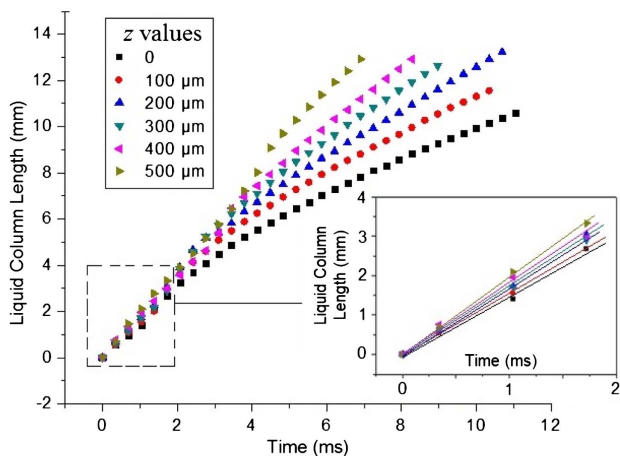

Fig. 3. (See Visualization 2) Formation and evolution of a liquid column formed by thermocavitation. The time interval between two images is 690 μs.

microscope slide's surface. Contrary to the liquid columns produced by LIFT, its dynamic is driven by the shock wave produced by the collapse of the bubble and not by the bubble itself as shown in Fig. 2.
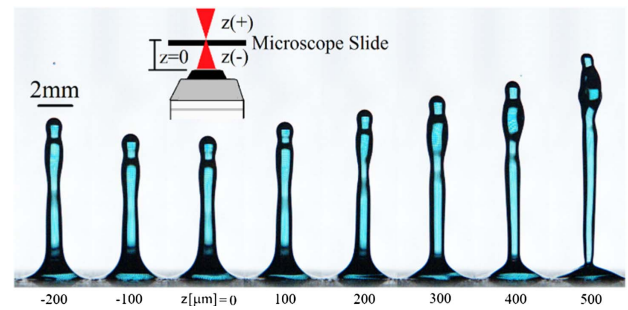
B. Aspect Ratio Λ

Our purpose is to show how thermocavitation produced within a droplet can be employed for the formation of liquid jets of controllable direction and with high aspect ratio that would be unstable otherwise. On the other hand, the length of the liquid column depends not only on the droplet's volume [32] but also on the ASW amplitude. However, the ASW is strongly related to the bubble's size, which can be controlled by adjusting the laser power or the distance between the beam focus point and the glass-liquid interface (variations in z). As the objective can be displaced vertically, the beam is focused at different positions from the interface (glass-liquid) and, thus, it changes the beam intensity at the interface. This controls the volume of superheated liquid available for evaporation and, thus, the amplitude of the ASW [41,42].

Figure 4 shows the temporal evolution of a liquid column length ejected from a 5 μL volume droplet at different z values. It is possible to observe that the column length and speed (see caption) become larger as the distance between the beam focus point and the interface (glass-liquid) increases. This occurs because the rate of energy deposition is smaller for lower light intensity; thus, the heat diffusion allows a larger superheated volume and, therefore, larger ASW [34,41,42]. This implies that a larger force is exerted on the liquid-air interface and therefore higher jet velocities result. In Fig. 5 we present eight liquid columns at the same time after the bubble collapse but at different z values (positive and negative). It is seen that the liquid column's length is almost symmetric around $z = 0$, because the intensity at the interface (glass-liquid) is symmetric too (see inset image in Fig. 5). Therefore, to obtain larger liquid columns it is necessary to increase or decrease the distance z. In each case, the length L and the diameter $2r$ of the column were
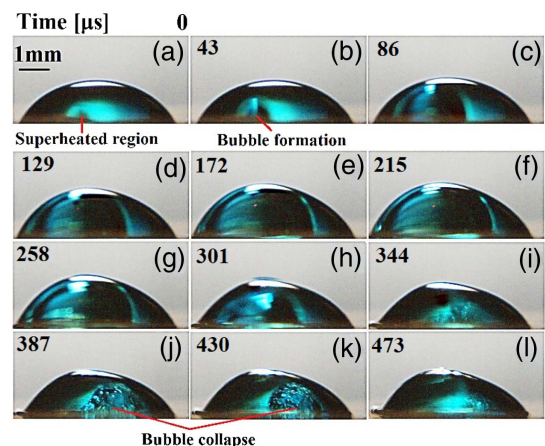

Fig. 5. Length of the liquid column at the same time (6.116 ms after the bubble collapse) but at different z values, for a droplet of 5 μL.

measured just before breaking up into droplets. The aspect ratio Λ values obtained for the columns from $z = 0$ to 500 μm in 100 μm intervals are 12.7, 13.5, 14.3, 14.7, 15.08, and 16, respectively. These values seem modest compared to those produced using the LIFT technique [27,28] (>100) but were produced with a novel mechanism of cavitation that employs CW lasers.

C. Ejection Angle of the Liquid Jet

Figure 6 shows the temporal evolution of a vapor bubble formed within a droplet when the laser focus position was placed to the left ($x = -400$ μm) of the droplet's symmetry center when the laser focus is at $z = 0$. The bubble grows and reaches its maximum radius deforming the left side of the droplet's surface [Fig. 6(f)]. From this point, the bubble begins to shrink. The asymmetry induced in the bubble causes a collapse to the right of the droplet's center [Fig. 6(j)]. It is possible to observe that the implosion point is almost symmetric with the formation point of the bubble, i.e., that the ASW is emitted at a distance of $x = +400$ μm from the center of the droplet.

Figure 7 shows a vapor bubble formed inside a 5 μL volume droplet. The beam focus was placed above the interface glass water ($z = 200$ μm) at different x values (0, –300, –600,

Fig. 4. Liquid column length as a function of time at different beam focus positions (z values). The inset shows a zoom to the initial part of the column's evolution. Solid lines indicate the initial velocity of the columns. The velocities obtained are 1.27, 1.44, 1.55, 1.7, 1.75, 1.96 m/s from $z = 0$ to 500 μm at 100 μm intervals, respectively.

Fig. 6. (See Visualization 3) Vapor bubble formed within a droplet of 5 μL of volume. The laser focus position was placed at $z = 0$ and $x = -400$ μm.
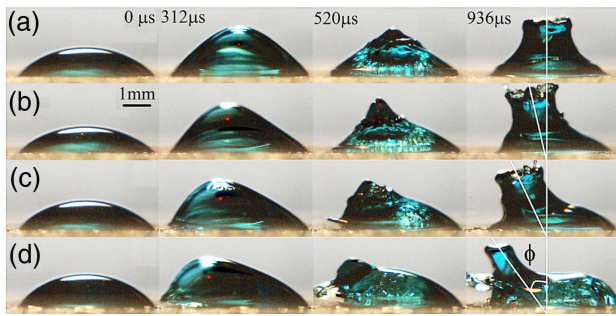
Fig. 7. Vapor bubble formed within a droplet of 5 μL of volume. The rows show pictures when the laser focus position was placed at (a) $x = 0$, (b) $x = -300$ μm, (c) $x = -600$ μm, and (d) $x = -900$ μm from the center of the droplet's base. For all cases, z was fixed to 200 μm. The columns show pictures at the same time.

and −900 μm). Since the bubble is generated at different positions inside the droplet, the ASW is also emitted at different positions on the glass-liquid interface. The ASW travels from its origin toward the water/air interface, reflecting and exerting a force on the surface. After this reflection, the ASW is reflected again on the substrate's surface and travels back to the water/air interface where it is focused. The force exerted by the ASW focused on the surface drives the formation of the liquid columns whose emitted angle ϕ changes with beam focus position.

Figure 8 shows the temporal evolution of the liquid jets generated under the same conditions as shown in Fig. 7 but with a wider field of view. As can be seen, the liquid column deviates from the vertical as the magnitude of x increases, but since the column is in contact with the droplet, the surface tension causes the ejection angle to change with time. Eventually, the column

detaches from the droplet, and the angle at the moment of detachment remains constant. However, its value is almost 4 times smaller than its initial value, reducing the ejection angle from ∼45° to ∼12°, for the cases when $x = -900$ μm. Nevertheless, this work shows the potential of ejecting liquid columns at different angles.
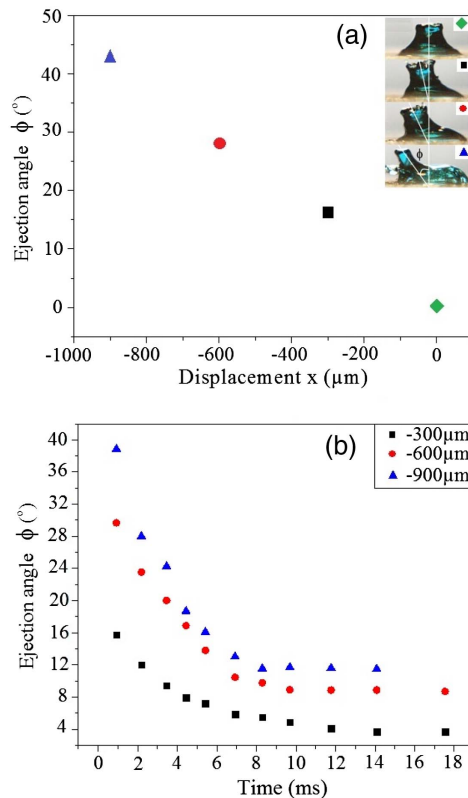
In Fig. 9, the initial ejection angle of the liquid column is plotted as a function of x. Here, it is possible to note that the initial ejection angle of the liquid column increases linearly as the distance between the center of the droplet's base and the horizontal position of the beam focus increases. At first glance, simply by varying x in an interval between −900 and +900 μm, it is possible to control the ejection angle from roughly −45° to +45°. Therefore, taking into account the radial symmetry of the droplet, the liquid column can be expelled in any direction within a cone of ∼90°. Outside this range, the vapor bubble breaks the surface tension and escapes by the droplet's side. The angle of the fully detached column, however, is almost a factor of 4 smaller compared to its initial angle due to surface tension.

4. SIMULATION AND DISCUSSION

From the experiment, it follows that the jet formation is a result of a shock wave action on the droplet surface. However, the exact propagation pattern is difficult to calculate because of two factors. First, the droplet shape at a moment of shock wave formation is modified by a previous bubble evolution, and it is not spherical and not even symmetric (Fig. 8). Second, the shock wave inside the drop experiences multiple rebounds resulting in the formation of caustics, and the wavefront shape even after a small number of rebounds becomes highly complicated. In terms of rays, the ray trajectories for the characteristic droplet shape become chaotic.
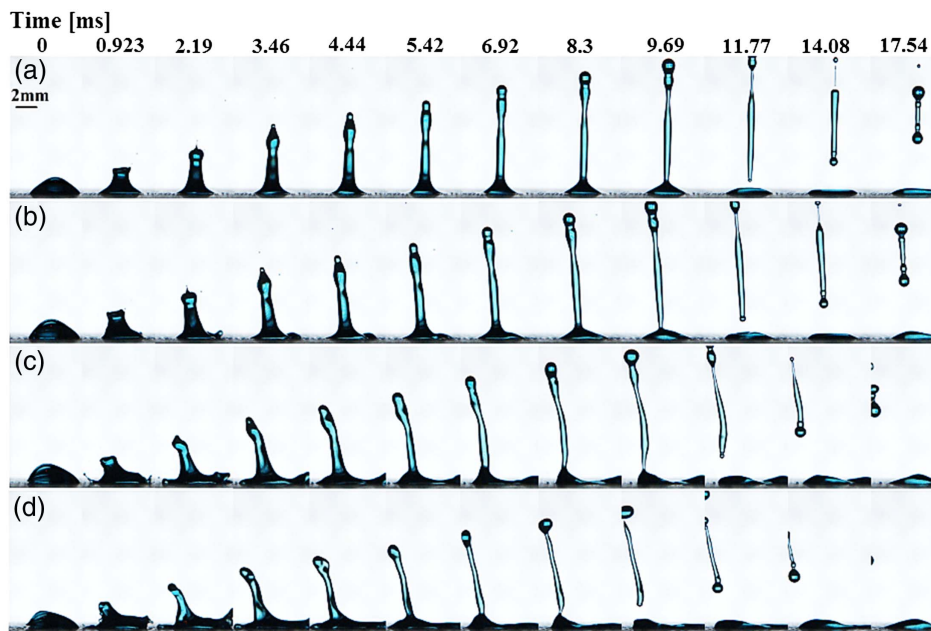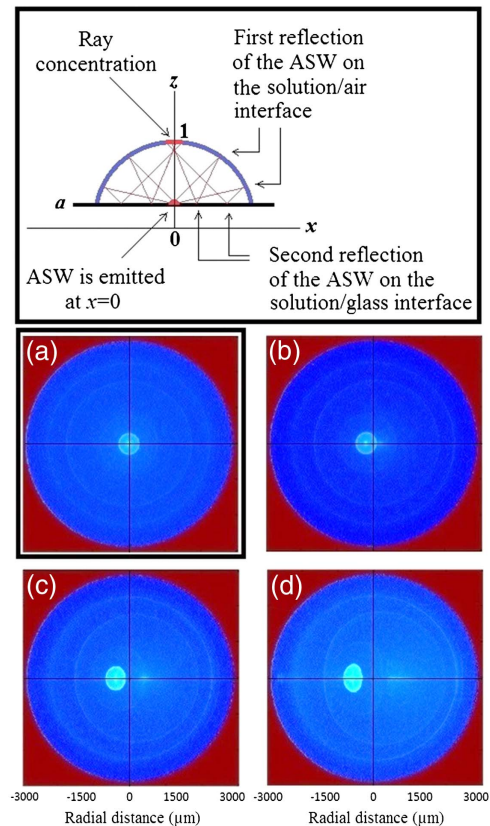

Fig. 8. Temporal evolution of liquid columns that emerge from a droplet of 5 μL volume at different x values, (a) $x = 0$ (See Visualization 4), (b) $x = -300$ μm (See Visualization 5), (c) $x = -600$ μm (See Visualization 6), and (d) $x = -900$ μm (See Visualization 7) from the center of the droplet's base.

Fig. 9. (a) Initial ejection angle of the liquid column as a function of the horizontal position of the beam focus (*x* parameter) and (b) its temporal evolution.

Fig. 10. Simulations of ray propagation at different *x* values, (a) $x = 0$, (b) $x = 300$ μm, (c) $x = 600$ μm, and (d) $x = 900$ μm from the center of the droplet's base. The clearest spot indicates focusing of the rays on the surface of the droplet (top view) in accordance with the experiment. The inset is a schematic representation (side view) of the droplet geometry and ray tracing just for illustration purposes [only for the case (a)].

Thus, for a simulation we limit ourselves to a simplified model, which, however, explains the focusing position of the shockwave and the general direction of jet emission. We assume a droplet spherical cap of radius $R_d = 1$ with its center at the origin and limited by a plane $z = a$, with $0 \leq a < 1$. Note that the parameter *a* determines the size and shape of the spherical cap. We further assume, that the energy is propagated along the paths of classic rays [45]. A large number *N* of rays, which start at the collapse point, with coordinates (x_0, y_0, a) are traced. We choose a uniform angular distribution (the probability to find a ray in any solid angle $d\Omega$ is proportional to $d\Omega$ and independent of the direction of the ray). The rays are perpendicular to the shock wavefront. The rays are reflected on the spherical cap according to the laws of geometrical optics. The momentum transfer from each ray to the surface is calculated, taking into account that after every rebound from the glass/droplet interface, 67% of energy is lost. We take into account eight rebounds for each ray, which gives 96% of total energy. In Fig. 10 the calculated momentum transfer to the surface is shown in color, bright areas corresponding to higher force. It is seen that after the first rebound on the spherical droplet/air interface the wave is focused and hits the surface in a spot, which is approximately opposite to the cavitation bubble position with respect to a center, as observed in the experiment. It is also seen that different caustics are formed, mainly due to a few first reflections (bright rings). Thus, the simulation suggests that most of the shock wave momentum is concentrated in a

relatively small spot, and a position of this spot qualitatively corresponds to the site where the jet appears. We stress that our model is highly simplified and does not permit a detailed comparison to an experiment but nevertheless predicts quite well the focusing position of the shockwave and the general direction of jet emission.

5. CONCLUSIONS

We have shown the generation and evolution of nozzle-free liquid jets of controllable direction produced within a $CuNO_4$ droplet by thermocavitation. The jets are driven by an acoustic shock wave emitted by the collapse of a hemispherical vapor bubble. The generated shock wave is reflected at the liquid-air interface due to an acoustic impedance mismatch generating multiple reflections inside the droplet. During each reflection, a force is exerted on the liquid-air interface driving the jets. Depending on the position of generation of the bubble within the droplet, the mechanical energy of the shock wave is focused on different regions at the liquid-air interface, ejecting cylindrical liquid jets at different angles. The ejected jet angle dependence is explained by a simple ray tracing model of the propagation of the acoustic shock wave inside the droplet.

REFERENCES

1. V. Goldshtein, I. Goldfard, I. Schrieber, and A. Zinovier, "Oscillations in a combustible gas bubble," Combust. Theory Modell. **2**, 1–17 (1998).
2. M.-A. Park, H.-J. Jang, F. V. Sirotkin, and J. J. Yoh, "Er:YAG laser pulse for small-dose splashback-free microjet transdermal drug delivery," Opt. Lett. **37**, 3894–3896 (2012).
3. J. Baxter and S. Mitragotri, "Needle-free liquid jet injections: mechanism and applications," Expert Rev. Med. Devices **3**, 565–574 (2006).
4. O. A. Basaran, "Small-scale free surface flows with breakup: droplet formation and emerging applications," AIChE J. **48**, 1842–1848 (2002).
5. G. D. Martin and I. M. Hutchings, "Inkjet printing—the physics of manipulating liquid jets and drops," J. Phys. **105**, 012001 (2008).
6. N. Bertin, R. Wunenburger, E. Brasselet, and J. P. Delville, "Liquid-column sustainment driven by acoustic wave guiding," Phys. Rev. Lett. **105**, 164501 (2010).
7. J. H. Lienhard V, "Liquid jet impingement," in *Annual Review of Heat Transfer*, C. L. Tien, ed. (Begell House, 1995), Vol. **6**, Chap. 4, p. 199.
8. W. Deng and A. Gomez, "Electrospray cooling for microelectronics," Int. J. Heat Mass Transfer **54**, 2270–2275 (2011).
9. J. Eggers and E. Villermaux, "Physics of liquid jets," Rep. Prog. Phys. **71**, 036601 (2008).
10. M. K. Tan, J. R. Friend, and L. Y. Yeo, "Interfacial jetting phenomena induced focused surface vibrations," Phys. Rev. Lett. **103**, 024501 (2009).
11. J. K. Luo, Y. Q. Fu, and W. I. Milne, *Acoustic Wave Based Microfluidics and Lab-on-a-Chip, Modeling and Measurement Methods for Acoustic Waves and for Acoustic Microdevices*, M. G. Beghi, ed. (InTech, 2013).
12. A. Patrascioiu, J. M. Fernández-Pradas, A. Palla-Papavlu, J. L. Morenza, and P. Serra, "Laser-generated liquid microjets: correlation between bubble dynamics and liquid ejection," Microfluid. Nanofluid. **16**, 55–63 (2014).
13. X. Chen, R. Xu, Z. Shen, J. Lu, and X. Ni, "Impact of a liquid-jet produced by the collapse of laser-induced bubbles against a solid boundary," Microw. Opt. Technol. Lett. **48**, 1525–1528 (2006).
14. E. Robert, J. Lettry, M. Farhat, P. A. Monkewitz, and F. Avellan, "Cavitation bubble behavior inside a liquid jet," Phys. Fluids **19**, 067106 (2007).
15. T. Tominaga, A. Nakagawa, T. Hirano, J. Sato, K. Kato, S. H. R. Hosseini, and K. Takayama, "Application of underwater shock wave and laser-induced liquid jet to neurosurgery," Shock Waves **15**, 55–67 (2006).
16. S. T. Thoroddsen, K. T. Takehara, G. Etoh, and C. D. Ohl, "Spray and microjets produced by focusing a laser pulse into a hemispherical droplet," Phys. Fluids **21**, 112101 (2009).
17. T. Lee, H. W. Baac, J. G. Ok, H. S. Youn, and L. J. Guo, "Nozzle-free liquid microjetting via homogeneous bubble nucleation," Phys. Rev. Appl. **3**, 044007 (2015).
18. J. Friend, "Microscale acoustofluidics: microfluidics driven via acoustics and ultrasonics," Rev. Mod. Phys. **83**, 647–704 (2011).
19. J. C. Carls and J. R. Brock, "Laser-induced breakout and detonation waves in droplets. II. Model," J. Opt. Soc. Am. B **8**, 329–336 (1991).
20. L. Heijnen, P. A. Quinto-Su, X. Zhao, and C. D. Ohl, "Cavitation within a droplet," Phys. Fluids **21**, 091102 (2009).
21. J. B. Zheng, W. F. Hsieh, S. Chen, and R. K. Chang, "Laser induced breakout and detonation waves in droplets. I. Experiments," J. Opt. Soc. Am. B **8**, 319–328 (1991).
22. M. S. Brown, N. T. Kattamis, and C. B. Arnold, "Time-resolved dynamics of laser-induced micro-jets from thin liquid films," Microfluid. Nanofluid. **11**, 199–207 (2011).
23. D. Obreschkow, P. Kobel, N. Dorsaz, A. Bosset, C. Nicollier, and M. Farhat, "Cavitation bubble dynamics inside liquid drops in microgravity," Phys. Rev. Lett. **97**, 094502 (2006).
24. R. Pohl, C. W. Visser, G.-W. Römer, D. Lohse, C. Sun, and B. Huis in 't Veld, "Ejection regimes in picosecond laser-induced forward transfer of metals," Phys. Rev. Appl. **3**, 024001 (2015).
25. C. Frederik Brasz, J. H. Yang, and C. B. Arnold, "Tilting of adjacent laser-induced liquid jets," Microfluid. Nanofluid. **18**, 185–197 (2015).
26. P. Delaporte and A.-P. Alloncle, "[INVITED] Laser-induced forward transfer: a high resolution additive manufacturing technology," Opt. Laser Technol. **78**, 33–41 (2016).
27. E. Biver, L. Rapp, A.-P. Alloncle, and P. Delaporte, "Multi-jets formation using laser forward transfer," Appl. Surf. Sci. **302**, 153–158 (2014).
28. M. Duocastella, J. M. Fernández-Pradas, J. L. Morenza, and P. Serra, "Time-resolved imaging of the laser forward transfer of liquids," J. Appl. Phys. **106**, 084907 (2009).
29. A. Pearson, E. Cox, J. R. Blake, and S. R. Otto, "Bubble interactions near a free surface," Eng. Anal. Bound. Elem. **28**, 295–313 (2004).
30. Y. Tagawa, N. Oudalov, C. Willem Visser, I. R. Peters, D. van der Meer, C. Sun, A. Prosperetti, and D. Lohse, "Highly focused supersonic microjets," Phys. Rev. X **2**, 031002 (2012).
31. C. Berrospe-Rodriguez, C. W. Visser, S. Schlautmann, R. Ramos-Garcia, and D. F. Rivas, "Continuous-wave laser generated jets for needle free applications," Biomicrofluidics **10**, 014104 (2016).
32. J. P. Padilla-Martinez, D. Banks, J. C. Ramirez-San-Juan, N. Korneev, G. Aguilar, and R. Ramos-Garcia, "Breaking the Rayleigh-Plateau instability limit using thermocavitation within a droplet," Atomization Sprays **23**, 487–503 (2013).
33. S. F. Rastopov and A. T. Sukhodolsky, "Sound generation by thermo-cavitation-induced cw laser in solutions," Proc. SPIE **1440**, 127–134 (1990).
34. J. C. Ramirez-San Juan, E. Rodriguez-Aboytes, A. E. Martinez-Canton, O. Baldovino-Pantaleon, A. Robledo-Martinez, N. Korneev, and R. Ramos-Garcia, "Time-resolved analysis of cavitation induced by CW lasers in absorbing liquids," Opt. Express **18**, 8735–8742 (2010).
35. J. P. Padilla-Martinez, C. Berrospe-Rodriguez, G. Aguilar, J. C. Ramirez-San-Juan, and R. Ramos-Garcia, "Optic cavitation with CW laser: a review," Phys. Fluids **26**, 122007 (2014).
36. J. C. Ramirez-San-Juan, E. Rodriguez-Aboytes, N. Korneev, O. Baldovinos-Pantaleon, R. Chiu-Zarate, G. Gutiérrez, R. Dominguez-Cruz, and R. Ramos-Garcia, "Cavitation induced by continuous wave lasers," Proc. SPIE **6644**, 66441M (2007).
37. P. Kafalas and A. P. Ferdinand, Jr., "Fog droplet vaporization and fragmentation by a 10.6-μm laser pulse," Appl. Opt. **12**, 29–33 (1973).
38. V. P. Skripov and P. A. Pavlov, "Explosive boiling of liquids and fluctuation nucleus formation," High Temp. **8**, 782–787 (1970); translated from Teplofiz. Vys. Temp. 8, 833–839 (1970).
39. O. Yavas, P. Leiderer, H. K. Park, C. P. Grigoropoulos, C. C. Poon, W. P. Leung, N. Do, and A. C. Tam, "Optical reflectance and scattering studies of nucleation and growth of bubbles at a liquid-solid interface induced by pulsed laser heating," Phys. Rev. Lett. **70**, 1830–1833 (1993).
40. F. Caupin and E. Herbert, "Cavitation in water: review," C. R. Phys. **7**, 1000–1017 (2006).
41. N. Korneev, P. Rodriguez-Montero, R. Ramos-Garcia, J. C. Ramirez-San-Juan, and J. P. Padilla-Martinez, "Ultrasound induced by CW laser cavitation bubbles," J. Phys. **278**, 012029 (2011).
42. J. P. Padilla-Martinez, G. Aguilar, J. C. Ramirez-San-Juan, and R. Ramos-Garcia, "Temporal evolution of thermocavitation bubbles using high speed video camera," Proc. SPIE **8097**, 809727 (2011).
43. J. C. Ramirez-San-Juan, J. P. Padilla-Martinez, P. Zaca-Moran, and R. Ramos-Garcia, "Micro-hole drilling in thin films with cw low power lasers," Opt. Mater. Express **1**, 598–604 (2011).
44. J. P. Padilla-Martinez, D. Banks, J. C. Ramirez-San-Juan, R. Ramos-Garcia, F. Sun, and G. Aguilar, "Towards the enhancement of transdermal drug delivery through thermocavitation," Photon. Laser Med. **1**, 183–193 (2012).
45. F. B. Jensen, W. A. Kuperman, M. B. Porter, and H. Schmidt, "Ray methods," in *Computational Ocean Acoustic*, 2nd ed., Modern Acoustics and Signal Processing (Springer-Verlag, 2011), p. 155.